

## Forced field ionization of Rydberg states for the production of monochromatic beams

E. Moufaret,<sup>1</sup> M. Vielle-Grosjean,<sup>1</sup> G. Khalili,<sup>1</sup> A. J. McCulloch,<sup>2</sup> F. Robicheaux,<sup>3</sup> Y. J. Picard,<sup>1</sup> and D. Comparat<sup>1</sup>  
<sup>1</sup>Laboratoire Aimé Cotton, CNRS, Université Paris-Sud, ENS Paris-Saclay, Université Paris-Saclay, Bât. 505, 91405 Orsay, France

<sup>2</sup>School of Physics, The University of Melbourne, Victoria 3010, Australia

<sup>3</sup>Department of Physics and Astronomy, Purdue University, West Lafayette, Indiana 47907, USA

(Received 4 November 2016; published 10 April 2017)

We study Rydberg ionization in an electric field in order to produce monochromatic ion and electron beams. We present an experimental study of the photoexcitation and ionization of high quantum-defect states, using excitation from the  $7s$  state in cesium to Rydberg states in the presence of a uniform electric field. Such states can exhibit complex ionization behavior, for instance, highly localized growth in the ionization rate due to interference effects. The data are well reproduced by the WKB quantum-defect and frame transformation methods with no adjustable parameters. This indicates that large changes in the Rydberg ionization rate from small changes in electric field are possible when a nearly stable state crosses a more unstable state. A fast variation of the ionization rate with electric field allows for the production of beams with very low energy dispersion. We develop a simple two-level model to predict the voltage and spatial resolution that would occur when atoms are prepared in a state with such sharp ionization in electric field. This confirms that Rydberg forced ionization in an electric field presents a pathway for the production of high-brightness, highly monochromatic ion and electron beams.

DOI: [10.1103/PhysRevA.95.043409](https://doi.org/10.1103/PhysRevA.95.043409)

### I. INTRODUCTION

Direct ionization or excitation of atoms has been used previously to produce monochromatic ion and electron beams [1–7]. We proposed in Ref. [8] a method for the production of highly monochromatic charged beams via excitation of Rydberg states in an atomic beam. The fundamental idea is to excite atoms from an atomic beam which will then enter an electric-field ionization region where they will be ionized. Ideally, all ions or electrons will be produced at the same voltage, leading to a monochromatic beam. For instance, a hypothetical  $v \approx 100$  m/s beam entering a region where the ionization rate rises abruptly to  $\Gamma \approx 10^9$  s<sup>-1</sup> will produce an ionization region of only  $\sim 0.1$   $\mu$ m. This value is well below what is achievable by direct focused laser photoionization (typically  $> 1$   $\mu$ m). In this article we present detailed theoretical and experimental results towards the realization of this idea by studying the ionization of Rydberg states in electric fields.

We first present a simple two-level model, valid for nonhydrogenic states with small quantum defects. It describes the basic physical process of stable states becoming unstable via a coupling to the continuum, as the electric field is modified. This allows us to extract general relations between the beam velocity, the ionization rate, the electric field gradient, and the energy dispersion of the final produced beam.

Secondly, we experimentally study the ionization of Cs Rydberg atoms for  $n \approx 25$  near the classical field ionization threshold for a field strength of  $F \approx 800$  V/cm. Due to the large quantum defect, the coupling between the stable and unstable states is more complex, and the experimental spectrum is compared to more elaborate multichannel quantum-defect theories [9,10]. Finally, we identify states that appear suitable for the production of monoenergetic ion or electron beams.

Figure 1 illustrates a possible realization of the scheme proposed in Ref. [8]. An atom is excited to a stable atomic state; then, due to the velocity  $v$  of the atomic beam, the atom will reach, at  $z = z_c$ , a “crossing” field  $F_c$  where it

becomes unstable, resulting in ionization. If the ionization occurs instantaneously, all ions and electrons will be produced in the exact same field environment and hence the formed beam will be monochromatic. Following previous work on Rydberg ionization in a beam traveling through an inhomogeneous field [11], we have recently excited a Cs beam to Rydberg states and have already demonstrated a higher ion yield compared to direct photoionization and an energy spread of the order of 1 eV, well below the 5 eV of commercial ion sources [12]. One of the goals of this article is to present a study of precision spectroscopy of Cs Rydberg states that may improve this result in the near future.

It is beyond the scope of this article to deal with the space-charge problem or electric field inhomogeneity, both of which can increase the energy dispersion of the beam. Some of these aspects have already been investigated in Ref. [8]. For example, states in the range  $n \approx 25$ –35 seem to be a good compromise between low  $n$  with smaller space-charge effects but larger energy dispersion, and high  $n$  with larger space-charge effects but smaller energy dispersion.

For simplicity we assume in this article that a one-dimensional beam propagates on axis with constant velocity. The ionization probability following the excitation of a single atomic state at time  $t_0$  (adiabatic assumption) can be calculated using the formula

$$P(z = z_c + vt) = 1 - e^{-\int_{t_0}^t \Gamma[F(z_c + vt')] dt'}, \quad (1)$$

where  $\Gamma(F)$  is the ionization rate at a given field  $F$ . For a constant field gradient  $\frac{dF}{dz}$  the formula (1) becomes

$$P[F(z)] = 1 - e^{-\frac{1}{v \frac{dF}{dz}} \int_{F_0}^{F(z)} \Gamma(F') dF'}, \quad (2)$$

from which we can extract the important considerations that a rapid variation of  $\Gamma(F)$  in electric field will help to produce a sharp variation of the ionization probability and thus produce a monochromatic beam.

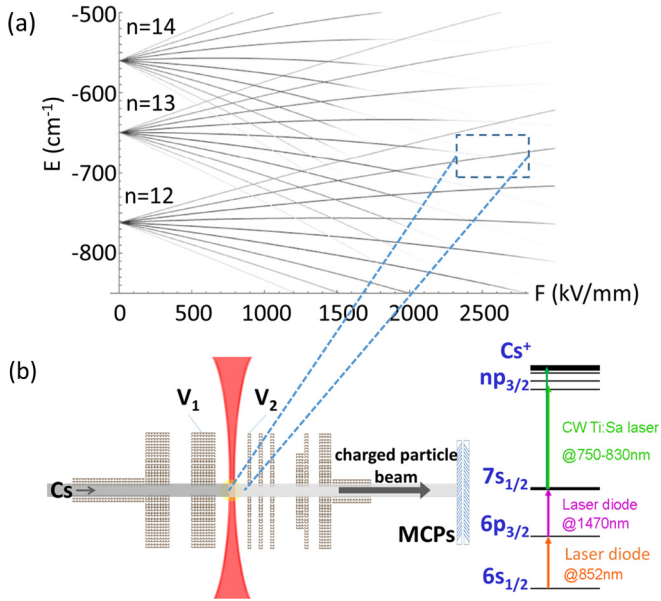


FIG. 1. Principle of ion or electron beam production using sharp Rydberg forced field ionization. Electrons and ions are produced by laser excitation of Rydberg states that are then field ionized. (a) Stark diagram (binding energy levels versus electric field) showing the slow Rydberg evolution toward its field ionization in the ( $|m| = 2$ ) hydrogen case. (The ionization rate is contrast coded and the dipole transition strength from an  $s$  state is intensity coded.) (b) Sketch of the experiment: an atomic beam is laser excited and then enters an inhomogeneous field where it is field ionized. In the case of alkali atoms, the ionization will be strongly affected near the crossing due to the core induced interaction between the states.

The velocity depends on the source, with typical values of  $v \approx 10$  m/s for a laser-cooled source,  $v \approx 100$ – $200$  m/s for a cryogenic beam, and  $v \approx 200$ – $2000$  m/s for a thermal or a supersonic beam. To give an order of magnitude in our numerical application we shall use  $v = 100$  m/s.

In Ref. [8], using analytical formulas for hydrogen atoms [13,14], the  $n \approx 30$  Rydberg state and an electric field gradient of  $\frac{dF}{dz} \approx 1$  (kV/mm)/mm, which is compatible with our experimental setup, it was shown that a beam dispersion of  $\Delta V \approx 0.1$  eV could be produced by a Rydberg forced field ionization occurring only in a micrometer spatial position. This energy dispersion is already better than any commercial electron or ion source.

Here, we proceed one step further by studying realistic models of state crossings (not necessarily adiabatic) that are valid for nonhydrogenic atoms, where the ionizing rate is not known *a priori*.

When several crossings are present, this can result in the mixing of amplitudes, producing interferences and multiple ionization thresholds [15–18]. The continuum itself can present sharp resonances due to reflection or interferences of waves above a potential barrier [17,19–21]. These effects may provide an interesting way to control the ionization. However, in order to get a simple physical picture we shall first restrict ourselves to a two-level isolated crossing such as in the zoomed part of Fig. 1(a) shown in Fig. 2(a).

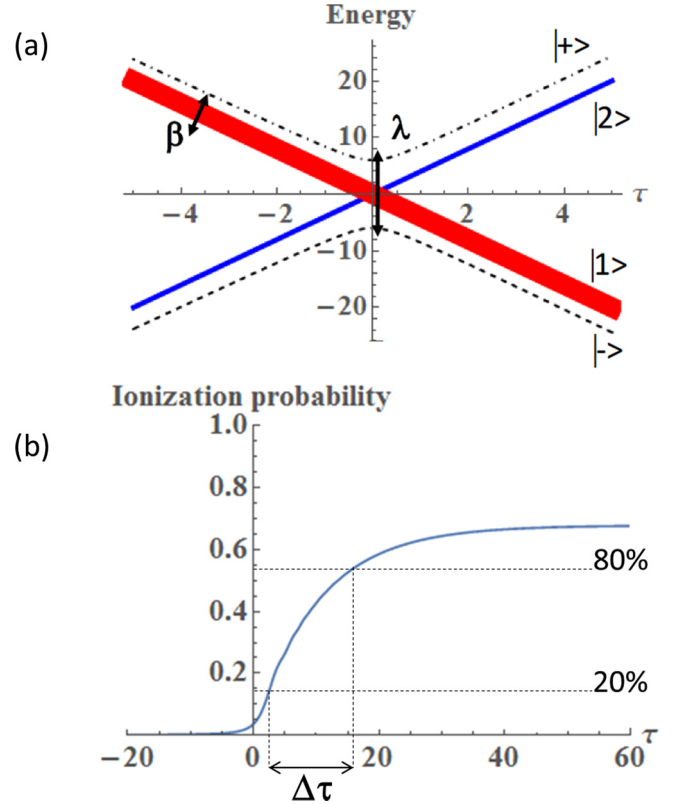


FIG. 2. Two-level crossing of a stable state  $|1\rangle$  (blue) coupled to an unstable one  $|2\rangle$  (red). (a) Sketch of the energy vs time (in dimensionless units) level crossing. The instability is represented by the linewidth  $\Gamma$  and the coupling is  $V = \hbar\Omega$ . The eigenstates  $|\pm\rangle$  are also represented. (b) Probability of ionization over the crossing: the solid curve is the exact solution of the decayed Landau-Zener. The two important parameters for the ionization are the final probability of ionization  $P(+\infty)$  and the ionization zone  $\Delta\tau_{20,80} = \Delta\tau$ , defined as being between 20% and 80% of the total ionization.

## II. SIMPLE FIELD IONIZATION MODEL

It is well known that the ionization of Rydberg states is different for hydrogen than for other atoms, such as the alkalis [17,22–24]. Indeed, alkali atoms typically ionize at the so-called classical field  $F = 1/16n^{*4}$  (in atomic units), where  $n^* = n - \delta_l$  is the effective quantum number that is linked to the binding energy of the states in zero field  $E = 1/2n^{*2}$ . Moreover, many of the Stark states of hydrogen with energies well above the classical ionization threshold can survive for times much longer than typical in an experiment. This is because the Hamiltonian for a nonrelativistic hydrogen atom in a uniform electric field separates in parabolic coordinates and the tunneling barrier is substantially different for different parabolic quantum numbers. As a shorthand, the hydrogenic states with substantially longer tunneling lifetimes will be referred to as “stable”.

The Hamiltonian of the valence electron of an alkali atom is that of hydrogen plus a perturbation due to core-polarization or spin-orbit effects:  $H = H_{\text{hydrogen}} + V_c$ . The atomic states are no longer the parabolic eigenstates  $|n, n_1, n_2, m\rangle$  (that we shall henceforth denote  $|n, n_1, m\rangle$ , since  $n = n_1 + n_2 + |m| + 1$ ) of the hydrogen atom in an electric field, since they are coupled

by the presence of the core. This perturbation strongly modifies the ionization properties of nonhydrogenic atoms (or molecules) compared to hydrogen atoms, and as such we can expect cases with a much sharper variation of ionization with  $F$ .

The simple picture shown in Fig. 2 explains ionization of a state  $|1\rangle$ , a stable  $|n, n_1, m\rangle$  state in the hydrogen case. It becomes unstable due to its crossing and coupling with an unstable state,  $|2\rangle = |n', n'_1, m'\rangle$ . The coupling matrix element will be denoted  $V = \langle n', n'_1, m' | V_c | n, n_1, m \rangle$ . This type of field ionization is typical of alkali atoms with low quantum defects, such as studied in the case of sodium with  $|m| = 2$  [25].

This two-level model, a stable level coupled to an unstable level with a lifetime of  $1/\Gamma$ , has been shown to accurately reproduce experimental data of Rydberg (auto-)ionization [11,25,26]. The effective Hamiltonian is

$$H(t) = \begin{pmatrix} E_1(t) & V \\ V & E_2(t) - i\hbar\Gamma/2 \end{pmatrix}. \quad (3)$$

Formulas to calculate the energy levels  $E_i(F)$  [27,28], the decay rate  $\Gamma(F)$  [13,28,29], and the coupling  $V$  [Eq. (A1)] can be used. The Schrödinger equation, the evolution of the state  $|\Psi\rangle = a_1(t)|1\rangle + a_2(t)|2\rangle$ , can be solved using experimental parameters to realistically model how the field  $F$  varies in time. This model has been successfully compared to experimental data Rydberg forced field ionization rate [11].

For the sake of simplicity we shall assume a linear variation of the field, i.e.,  $F(z) = \frac{dF}{dz}(z - z_c) + F_c$ , as well as a linear variation of the energy levels. We also assume that near the crossing the coupling  $\Gamma$  can be taken as constant  $\Gamma = \Gamma(F_c)$ . Important physical interpretations can be extracted from this so-called dissipative, decayed, or lossy Landau-Zener model:

$$H(t) = \frac{\hbar}{2} \begin{pmatrix} \alpha t & 2\Omega \\ 2\Omega & -\alpha t - i\Gamma \end{pmatrix}, \quad (4)$$

where  $E_1(t) - E_2(t) = \hbar\alpha t$  is linear in time, the coupling  $V = \hbar\Omega$ , and decay rate  $\Gamma$  are constants. This Hamiltonian can be simplified when using reduced dimensionless parameters: time  $\tau = t/\xi$ , adiabaticity  $\lambda = \xi\Omega$ , and decay  $\beta = \xi\Gamma$ , where  $\xi = 1/\sqrt{2\alpha}$ . The Hamiltonian, for the evolution equation  $i\frac{d\Phi}{d\tau} = H_\alpha\Phi$  of the wave function  $\Phi(\tau) = \Psi(t)$  becomes

$$H_\alpha(\tau) = \begin{pmatrix} \tau/4 & \lambda \\ \lambda & -\tau/4 - i\beta/2 \end{pmatrix}, \quad (5)$$

which has been extensively studied [30–39]. The time evolution is simply given by the analytical continuation of the standard Landau-Zener problem (without decay). We are interested in the ionization probability  $P(t) = 1 - (|a_1|^2 + |a_2|^2)$  [or similarly, by the survival probability  $1 - P(t)$ ], where analytical formulas have been derived for arbitrary time evolution [34,38,39]. However, because we assume an isolated crossing, we shall calculate the evolution starting with  $a_1(-\infty) = 1$  and  $a_2(-\infty) = 0$  [40].

One of the most intriguing properties of the lossy Landau-Zener model is that the long-time survival probability is independent of the decay rate  $\Gamma$  [32]. The first important physical result is that the irreversible decay does not affect the probability of ionization, which is still given by the Landau-Zener formula:

$$P(t \rightarrow +\infty) = 1 - e^{-\frac{2\pi\Omega^2}{\alpha}} = 1 - e^{-4\pi\lambda^2}. \quad (6)$$

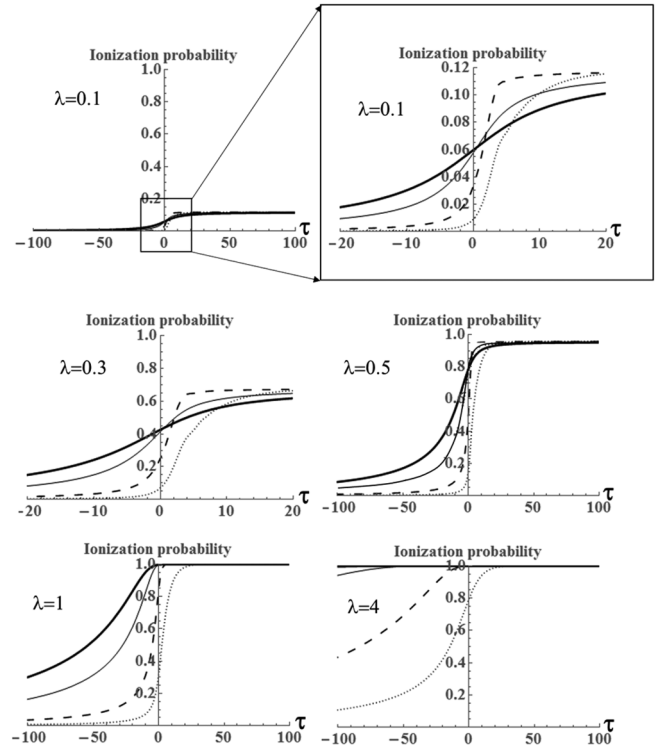


FIG. 3. Evolution of the ionization probability in the lossy Landau-Zener model for  $\beta = 0.2$  (dotted line),  $\beta = 1$  (dashed line),  $\beta = 5$  (thin line), and  $\beta = 10$  (broad line) in all cases, where  $\lambda = \Omega/\sqrt{2\alpha}$ ,  $\tau = t\sqrt{2\alpha}$ , and  $\beta = \Gamma/\sqrt{2\alpha}$ . The horizontal axis that represents the dimensionless time  $\tau$  is defined through  $\Gamma t = \beta\tau$ .

The case  $\lambda \gg 1$  is interesting because full ionization is achieved [ $P(t \rightarrow +\infty) \approx 1$ ] and, as is the case for the standard Landau-Zener, the transition is adiabatic in the sense that during the process only the adiabatic state  $|-\rangle$  is populated [39].

For such adiabatic evolution, the ionization probability is given by Eq. (1), which becomes  $P(t) = 1 - e^{-\int_{-\infty}^t \text{Im}[-2\epsilon_-(t')] dt'}$ , where  $\hbar\epsilon_{\pm}(t) = \frac{\hbar}{4} [-(2\alpha t + i\Gamma) \pm \sqrt{16\Omega^2 + (2\alpha t + i\Gamma)^2}]$  are the complex eigenvalues of the states  $|\pm(t)\rangle$ , with the proper analytical continuation of the square root. Obviously, this approximation is poor for nonadiabatic transitions, and in this case other formulas should be used, such as the one proposed in Ref. [11].

Additional to the ionization probability, the “slope”, or gradient of  $P$  with respect to  $F$ , is another important parameter. We want to have a fast variation of  $P(F[z(t)])$ , in order to have a small field variation during the ionization and thus a small energy dispersion. In order to gain quantitative insight into the length scale of ionization, we have defined the ionization zone  $\Delta z_{20,80}$  as the region between 20% and 80% of the full ionization. Therefore the energy dispersion can be estimated as the voltage difference in this zone to be  $\Delta V \approx F_c \Delta z_{20,80} = F_c v \Delta t = F_c v \xi \Delta \tau$ . We have plotted the numerical time evolution of the ionization for several ranges of the parameters in Fig. 3 [40]. This is the basic tool to estimate the energy dispersion in an experiment. For a given experimental realization, the results in Fig. 3 guide the choice of the appropriate states (lifetime and coupling) and

field gradient to optimize the ionization process: ionization efficiency and energy dispersion  $\Delta V$ .

The final ionization efficiency only depends on  $\lambda$ , as predicted in Eq. (6). The width  $\Delta\tau = \Delta\tau_{20,80}$ , as defined in Fig. 2, depends on the decay rate  $\beta$  (or  $\Gamma$ ) of the unstable state but also on the coupling strength  $\lambda$  (or  $\Omega$ ) between the states. At low coupling,  $\lambda < 1$ , the stable state is affected by the unstable state when their energies are similar. Because the energy of the unstable state can be seen as broadened by the decay rate  $\beta$ , we find that the broadening is thus mainly given by  $\beta$ . For large coupling,  $\lambda > 1$ , the adiabatic behavior dominates: the crossing between the states starts early, leading to a large width. For large decay, full ionization can occur before reaching the crossing. A low decay leads to a transfer of population toward the unstable state, allowing time for decay and also resulting in a large width.

We have, to first order (with  $k = n_1 - n_2 = 2n_1 - n - |m|$ )  $\alpha t = \frac{3}{2}(nk - n'k')\frac{dF}{dz}vt$ . A rough estimation is then  $\alpha \approx n^2\frac{dF}{dz}v$  or  $\xi \approx 1/n\sqrt{v\frac{dF}{dz}}$ , leading to

$$\lambda = \xi\Omega \approx 10\delta_{|m|}(n/34)^{-5}\left(\frac{100\text{ m/s } 10^9\text{ V/m}^2}{v\frac{dF}{dz}}\right)^{1/2}, \quad (7)$$

$$\beta = \xi\Gamma \approx \frac{1}{n}\left(\frac{100\text{ m/s } 10^9\text{ V/m}^2}{v\frac{dF}{dz}}\right)^{1/2}\frac{\Gamma}{10^8\text{ s}^{-1}}, \quad (8)$$

where we have used the approximate formula (see Appendix), in atomic units,  $\Omega \approx \frac{\delta_{|m|}}{n^4}$ .

We wish to emphasize that this two-level model is valid only if the two states are well separated from the others. This requires the coupling  $\Omega$  and linewidth  $\Gamma$  being smaller than the energy separation with surrounding levels. Because the Stark effect splits levels (on the same manifold) by  $\sim \frac{3}{2}nF_c$  and that we work near the classical ionization threshold  $F_c \approx 1/16n^4$ , we found that the model shall mainly be restricted to low quantum defects ( $\delta_{|m|} \ll n/10$ ) and to

$$\Gamma \leq (n/34)^{-3}10^{11}\text{ s}^{-1}. \quad (9)$$

The ionization efficiency and the energy dispersion  $\Delta V$  can be optimized using the experimental parameters  $\frac{dF}{dz}$  and  $\Gamma$  that can be largely tuned. (By a proper choice of  $n', k'$  values of the unstable state,  $\Gamma$  can be chosen in the range  $10^5 - 10^{11}\text{ s}^{-1}$  [23].) Complete ionization requires  $\lambda \approx 0.5$ . (A higher value will broaden the ionization region with no gain.) Assuming a value of  $\delta_{|m|} \approx 0.1$  and  $n > 34$ , Eq. (7) indicates that to have a complete ionization, the optimal value  $\lambda \approx 0.5$  can always be achieved for electric field gradients less than the maximum value of  $10^9\text{ V/m}^2$ . However, such complete ionization is not always compatible with the lowest possible energy dispersion. Indeed, a low  $\Delta V \approx F_c v \Gamma^{-1} \beta \Delta\tau$  requires a fast ionization rate  $\Gamma$  but also  $\beta < 0.5$  (Fig. 3 clearly indicates large  $\Delta t$  for higher values) and thus a maximum electric field gradient value of  $10^9\text{ V/m}^2$  [see Eq. (8)].

As an example, with  $n = 34$  and  $m = 3$  state of Cs ( $\delta_3 = 0.03$ ), a gradient of  $dF/dz \approx 10^9\text{ V/m}^2$  will produce a complete ionization, and by choosing a coupling with a state with  $\Gamma \approx 10^9\text{ s}^{-1}$ , this leads to an ionization time  $\Delta t \approx \Gamma^{-1}$  of only 1 ns, an ionization zone of only  $\Delta z = v\Delta t \approx 100\text{ nm}$ , and thus an energy dispersion of  $\Delta V = F_c \Delta z \approx 3\text{ meV}$ .

With  $n = 100$ , the smallest energy dispersion will be obtained for a coupling with a state with the highest possible decay rate of  $\Gamma \approx 4 \times 10^9\text{ s}^{-1}$  [see Eq. (9)], and a gradient  $dF/dz \approx 10^9\text{ V/m}^2$ , in order to keep  $\beta < 0.5$  [see Eq. (8)] which produces  $\Delta V \approx F_c v \Gamma^{-1} \approx 7\text{ }\mu\text{eV}$  but with an ionization efficiency of only 0.001%. A compromise with a decay rate of  $\Gamma \approx 5 \times 10^7\text{ s}^{-1}$  and a gradient  $dF/dz \approx 10^5\text{ V/m}^2$  would lead to 10% ionization efficiency and a sub-meV energy dispersion.

### III. IONIZATION OF CS RYDBERG STATES

The previous section gives a qualitative discussion of the values of parameters needed to obtain an ion or electron beam with a small energy spread. In this section, we report the results of experiments and more sophisticated calculations to show that specific states can be found with promising characteristics. For this, we have investigated the lifetime of Rydberg states for a fixed electric field using a Cs beam from a simple effusive recirculating oven with a similar setup as described in Ref. [12].

Laser excitation is performed by a three-step ( $6s(F=4) \rightarrow 6p_{3/2}(F=5) \rightarrow 7s(F=4) \rightarrow np$ ) excitation, the last two lasers being crossed orthogonally and having polarizations parallel to the field [41]. We can thus only excite  $m = 0$  states ( $m = 1/2$  taking into account the spin). In the case of Cs:  $\delta_0 \approx 4.05, \delta_1 \approx 3.6, \delta_2 \approx 2.5, \delta_3 \approx 0.03$  [42–44], and therefore we cannot use the simplified two-level theory presented in the previous section to evaluate the couplings between the states. Several approaches could have been employed for providing excitation towards states with  $m > 2$ , allowing use of this theory, such as adiabatic microwave transfer [45], circularly polarized microwave [46], or crossed (magnetic and electric) fields [47]. However, implementation of these methods would require alteration to the experimental apparatus.

A schematic of the experiment is shown in Fig. 1, except that the field is homogeneous. The Cs beam enters a DC electric field produced by plates separated by  $\sim 5\text{ mm}$ . Residual inhomogeneity of the electric field limits our spectral experimental resolution to  $\sim 50\text{ MHz}$  for states having the strongest Stark shifts with electric fields. Produced electrons are accelerated by the field to a double-stack microchannel plate (MCP) followed by a phosphor screen.

The laser waists are on the order of tens of micrometers. The laser powers (respectively  $\sim 10\text{ }\mu\text{W}$  for 852 nm,  $\sim 100\text{ }\mu\text{W}$  for 1470 nm, and 10 mW for the Rydberg excitation) are chosen to not significantly power broaden the lines. The Rydberg excitation ( $7s \rightarrow np$ ) laser is a Ti:Sa, the wavelength of which is monitored using a high-precision wavemeter (highfinesse WSU-2).

Figure 4 shows a theoretical map of the Stark states produced near the ionization threshold of  $F = 800\text{ V/cm}$  for  $n \approx 25$ . The photoabsorption theory is based on WKB quantum defect [9]. For this method, a local frame transformation is performed between the wave functions near the core that are well described by phase-shifted, spherical Coulomb functions, and the wave functions at large distances that are well described by the solutions of the Coulomb plus Stark potential in parabolic coordinates. In this method, there is a transformation matrix that depends only on the strength of the electric field. The specific properties of the atoms are incorporated through the zero-field quantum defects and

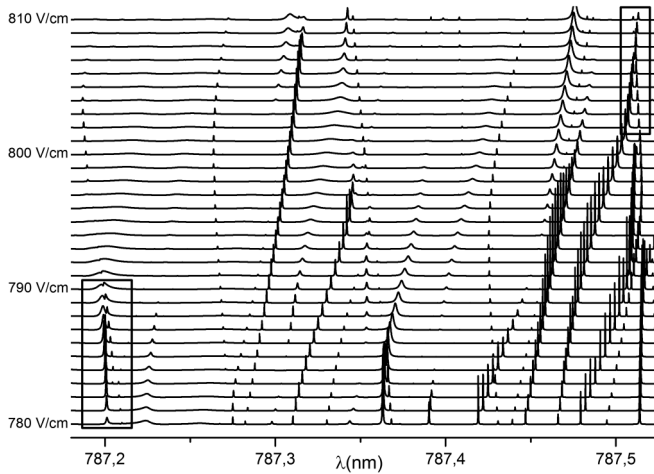


FIG. 4. Theoretical photoabsorption spectra for Cs excitation corresponding to an excitation from an  $s$  state with a  $\pi$  polarization (from  $l = 0$  and towards  $m = 1/2$ ). The rectangle areas are the one studied experimentally and zoomed in Figs. 5 and 6.

transition dipole matrix elements of the atom. The zero-field quantum defects are accurately known from experiments, and the transition dipole matrix elements can be obtained from effective one-electron potentials. The resonance lifetimes are obtained in this theory through the scattering between the different parabolic channels which occurs because the low-angular-momentum partial waves have a phase shift. Due to the complications of the theory, the trends in the resonance linewidths are obtained by a series of calculations with slightly different field strengths. A more exact theory, based on R-matrix local frame transformation [10], has been established, but we found the former one accurate enough for our purpose.

From this theoretical map, we identified several interesting states (typically one every V/cm in our region of 800 V/cm) that rapidly destabilize when the electric field is modified. We thus focused on experimentally finding such states. The electron signal is recorded when scanning the Ti:Sa frequency at a given electric field which is calibrated by comparison with the theory. We present a few of them in Figs. 5 and 6.

We are able to collect electrons even when a stable Rydberg state is excited. These electrons come from a subsequent photoionization by the Ti:Sa laser and are therefore produced with an excess energy of  $\sim 1$  eV. Thus, for small acceleration fields, some electrons do not reach the detector due to the large transverse momentum. This effect is clearly visible as a broadening of the electron spot size on the MCPs compared to electrons produced by direct photoionization or excitation to an unstable state, which creates electrons with near zero kinetic energy. It is possible to overcome this problem by reversing the voltage and collecting ions with the MCP, but the signal to noise is much lower at such low ion energies. However, as shown below, comparisons with theoretical photoabsorption spectra are quite good. Therefore, we can conclude that the signal intensity is not significantly affected by the Rydberg photoionization [48]. This is confirmed by simulations performed with SIMION software. Consequently, we use the peak intensity as a quantitative measurement of the excitation efficiency.

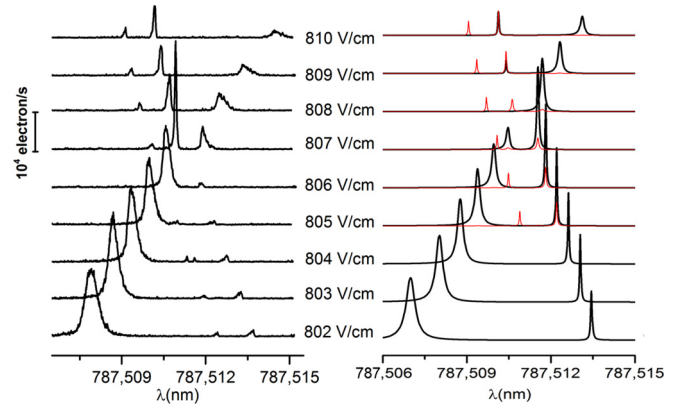


FIG. 5. Scan of ionization versus wavelength for varying field around a level crossing. Top: experimental data, where ejected electrons are collected. Bottom: theoretical photoabsorption spectra with excitation toward  $|m| = 1/2$  in the black thick line and  $|m| = 3/2$  in the red thin line with intensity divided by 30.

### A. Level crossing

The states shown in Fig. 5 illustrate the two-level model we presented in Sec. II. A stable (narrow) level is observed to cross an unstable (broad) one and the interaction between them results in instability. However, the situation appears slightly more complex because we observe also interference

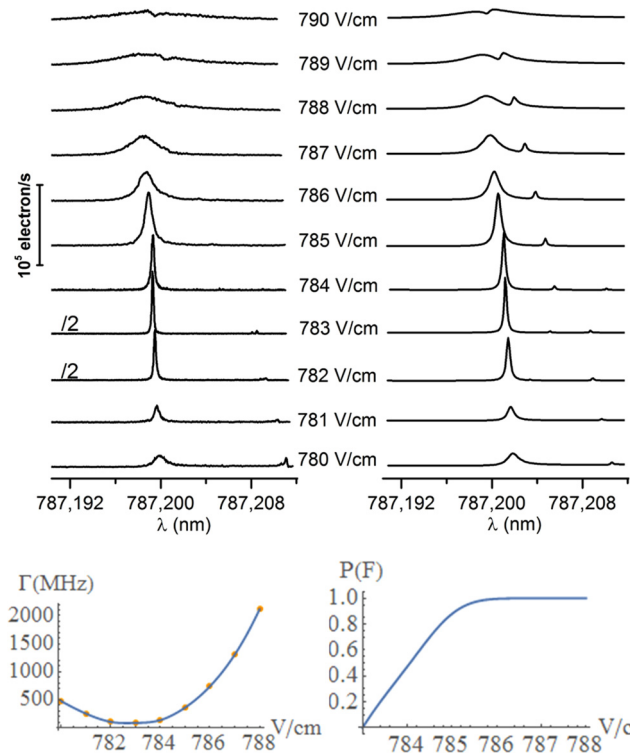


FIG. 6. Scan of ionization rate versus wavelength for varying field, displaying interference narrowing. Left: experimental data and theoretical spectra. (The intensity signal for scans at 782 V/cm and 783 V/cm have been half reduced to avoid overlap.) Right: Theoretical linewidth evolution in electric field and its interpolation used to plot the ionization probability if starting from 783 V/cm and traveling in a  $10^9$  V/m<sup>2</sup> gradient at 100 m/s.

effects with states with  $|m| = 3/2$  due to our imperfect parallel polarization to the field. The lifetime of the states is directly given by the inverse of the linewidth when scanning the laser frequency. Our experimental resolution of 50 MHz limits our measurement of long-lived states. We could have overcome this limitation by using a delayed pulsed electric field [23], but we more simply rely on the theory to extract linewidths below 50 MHz. We have not performed any convolution of the theoretical curves with the experimental resolution.

It is beyond the scope of this article to study in more detail the dynamical evolution of such complex crossing, and the lossy Landau-Zener two level model with a single decaying state can be questionable. However, it seems clear that a stable state crossed abruptly a state with linewidth of the order of 50 MHz. Therefore, using such a state to produce a charged particle beam should lead to an energy dispersion  $\Delta V = Fv\Gamma^{-1}$  on the order of tens of meV.

### B. Interference narrowing

A second example of stable Rydberg states becoming unstable can be seen in Fig. 6 where the standard Fano profile line shapes appears [49,50].

Here an unstable state becomes stable before once again becoming unstable. Such interference narrowing, resulting in a strong reduction in the ionization rate, has been observed in many Rydberg systems (see, for instance, [9,51–58]). One of the sharpest states ever observed was in He, where the ionization rate of the  $|35,5,29,0\rangle$  state near the field  $F_c \approx 467.5$  V/cm in He increases from few  $10^6$  s $^{-1}$  to  $5 \times 10^9$  s $^{-1}$  within a field range of  $\sim 0.1$  V/cm [58].

The simplest explanation of this phenomenon is given when two unstable states 1 and 2, both decaying toward the same continuum, interact together. The presence of this continuum can be seen as a third level that can produce a dark eigenstate (a state that has no continuum component) [59]. Therefore, even when two states 1 and 2 are unstable, their interaction can result in stabilization, producing a stable state [60]. In the case of cesium such interference effects have been reported in Refs. [50,55] but due to interaction with a quasicontinuum formed by a Stark manifold. If this is the first observation of an interference narrowing effect in cesium this is only because of lack of research and not because this effect is rare. On the contrary, we found theoretically that such a narrowing effect is quite common (we found a few of them in the region of Fig. 5), but an almost perfect narrowing effect is obviously rarer. Despite the difficulties to simulate such interference effects, the theory and experiment agree quite well (except for a small discrepancy for the largest field spectra). Such an ideal narrowing effect can be used to excite a stable state that will then be ionized efficiently when the field is varied. Study of such excitation has been performed in Refs. [53,60,61]. In our case the decay rate evolution can simply be inserted into Eq. (2). This gives an ionization size of only 1 V/cm in the gradient of  $10^5$  (V/cm)/cm, yielding  $\Delta z_{20,80} \approx 0.1 \mu\text{m}$  and thus an energy dispersion of  $F_c \Delta z_{20,80} \approx 10$  meV.

## IV. CONCLUSION

In Ref. [8] we claim that using forced field ionization of Rydberg states of nonhydrogenic atoms “leads to an

improvement of a factor 10 [compared to the hydrogen case] for the energy dispersion. It means that use of these special Rydberg states would result in a dramatic improvement of the characteristics of our source.” In this article we have confirmed this fact and have shown that further improvements could be made. For low quantum defects (for instance, for He, Li, or Na atoms), we have proposed a scheme to choose the best state in terms of slope in electric field, coupling with other states and lifetimes. The use of states with large  $n$  will produce very low energy dispersion beams.

Experiments with high quantum defects were performed in Cs and compare well with theory. Despite the strong coupling occurring between such states, it is possible to find states that ionize sharply in electric fields.

The next important step will be to achieve a well-defined transition from the excitation of a stable state in an electric field to higher (or lower) field values where the atom decays more rapidly [11]. This should open the path to the production of high-brightness, highly monochromatic ion and electron beams.

## ACKNOWLEDGMENTS

The research leading to these results has received funding from the European Research Council under Grant Agreement No. 277762 COLDNANO and ANR/DFG HREELM. This work was supported by the U.S. Department of Energy, Office of Science, Basic Energy Sciences, under Award No. DE-SC0012193, and the Australian Research Council Discovery through Project No. DP140102102. The authors also thank Sadiq Rangwala for active participation through the CEFIPRA Project, No. 5404-1.

## APPENDIX

### Coupling

For hydrogenic spherical states, the coupling is given by the formula  $\langle nlm|V_c|n'l'm'\rangle = \frac{-\delta_l}{\sqrt{n^3 n'^3}} \delta_{ll'} \delta_{mm'}$  [14,17]. When using the hydrogenic parabolic states as a basis set, it becomes

$$\langle nn_1m|V_c|n'n'_1m\rangle = \sum_l \langle nn_1m|nlm\rangle \frac{-\delta_l}{\sqrt{n^3 n'^3}} \langle n'l'm|n'n'_1m\rangle, \quad (\text{A1})$$

where we used completeness,  $\langle a|V|a'\rangle = \sum_{b,b'} \langle a|b\rangle \langle b|V|b'\rangle \langle b'|a'\rangle$ , to obtain this result. It is well known [17] that the projection  $\langle nn_1m|nlm\rangle$  is simply a Clebsch-Gordan coefficient  $|\langle nn_1m|nlm\rangle| = \sqrt{2l+1} \begin{pmatrix} \frac{n-1}{2} & \frac{n-1}{2} & l \\ m+n_1-n_2 & m-n_1+n_2 & m \end{pmatrix}$  on the order of  $1/\sqrt{n}$ .

Using the fact that the quantum defects decrease with  $l \geq |m|$ , we find a simple approximate formula

$$\langle nn_1m|V_c|n'n'_1m\rangle \approx \frac{-\delta_{|m|}}{n^2 n'^2}$$

that can even be approximated by

$$\langle nn_1m|V_c|n'n'_1m\rangle \approx \frac{-\delta_{|m|}}{n^4}.$$

- [1] A. C. Gallagher and G. York, A photoionization source of monoenergetic electrons, *Rev. Sci. Instrum.* **45**, 662 (1974).
- [2] F. B. Dunning, Electron-molecule collisions at very low electron energies, *J. Phys. B* **28**, 1645 (1995).
- [3] B. Ward, J. A. Notte, and N. P. Economou, Helium ion microscope: A new tool for nanoscale microscopy and metrology, *J. Vac. Sci. Technol. B* **24**, 2871 (2006).
- [4] V. L. Sukhorukov, I. D. Petrov, M. Schäfer, F. Merkt, M.-W. Ruf, and H. Hotop, Photoionization dynamics of excited Ne, Ar, Kr, and Xe atoms near threshold, *J. Phys. B* **45**, 92001 (2012).
- [5] M. Kitajima, M. Kurokawa, T. Kishino, K. Toyoshima, T. Odagiri, H. Kato, K. Anzai, M. Hoshino, H. Tanaka, and K. Ito, Ultra-low-energy electron scattering cross section measurements of Ar, Kr, and Xe employing the threshold photoelectron source, *Eur. Phys. J. D* **66**, 130 (2012).
- [6] J. J. McClelland, A. V. Steele, B. Knuffman, K. A. Twedt, A. Schwarzkopf, and T. M. Wilson, Bright focused ion beam sources based on laser-cooled atoms, *Appl. Phys. Rev.* **3**, 011302 (2016).
- [7] A. J. McCulloch, B. M. Sparkes, and R. E. Scholten, Cold electron sources using laser-cooled atoms, *J. Phys. B* **49**, 164004 (2016).
- [8] L. Kime, A. Fioretti, Y. Bruneau, N. Porfido, F. Fuso, M. Viteau, G. Khalili, N. Šantić, A. Gloter, B. Rasser, P. Sudraud, P. Pillet, and D. Comparat, High-flux monochromatic ion and electron beams based on laser-cooled atoms, *Phys. Rev. A* **88**, 033424 (2013).
- [9] D. A. Harmin, Analytical study of quasidiscrete Stark levels in Rydberg atoms, *Phys. Rev. A* **30**, 2413 (1984).
- [10] P. Giannakeas, C. H. Greene, and F. Robicheaux, Generalized local-frame-transformation theory for excited species in external fields, *Phys. Rev. A* **94**, 013419 (2016).
- [11] W. van de Water, D. R. Mariani, and P. M. Koch, Ionization of highly excited helium atoms in an electric field, *Phys. Rev. A* **30**, 2399 (1984).
- [12] M. Viteau, M. Reveillard, L. Kime, B. Rasser, P. Sudraud, Y. Bruneau, G. Khalili, P. Pillet, D. Comparat, I. Guerri, A. Fioretti, D. Ciampini, M. Allegrini, and F. Fuso, Ion microscopy based on laser-cooled cesium atoms, *Ultramicroscopy* **164**, 70 (2016).
- [13] R. J. Damburg and V. V. Kolosov, A hydrogen atom in a uniform electric field, III, *J. Phys. B: At. Mol. Phys.* **12**, 2637 (1979).
- [14] M. Forre, H. M. Nilsen, and J. P. Hansen, Dynamics of a H(n) atom in time-dependent electric and magnetic fields, *Phys. Rev. A* **65**, 053409 (2002).
- [15] T. H. Jeys, G. W. Foltz, K. A. Smith, E. J. Beiting, F. G. Kellert, F. B. Dunning, and R. F. Stebbings, Diabatic Field Ionization of Highly Excited Sodium Atoms, *Phys. Rev. Lett.* **44**, 390 (1980).
- [16] G. B. McMillan, T. H. Jeys, K. A. Smith, F. B. Dunning, and R. F. Stebbings, High-resolution field ionisation of Na(ns, nd) Rydberg atoms, *J. Phys. B* **15**, 2131 (1982).
- [17] T. F. Gallagher, *Rydberg Atoms* (Cambridge University Press, Cambridge, 1994).
- [18] R. Feynman, J. Hollingsworth, M. Vennettilli, T. Budner, R. Zmiewski, D. P. Fahey, T. J. Carroll, and M. W. Noel, Quantum interference in the field ionization of Rydberg atoms, *Phys. Rev. A* **92**, 043412 (2015).
- [19] R. R. Freeman, N. P. Economou, G. C. Bjorklund, and K. T. Lu, Observation of Electric-Field-Induced Resonances Above the Ionization Limit in a One-Electron Atom, *Phys. Rev. Lett.* **41**, 1463 (1978).
- [20] E. Luc-Koenig and A. Bachelier, Interpretation of Electric-Field-Induced Oscillations in the Cross Section of a One-Electron Atom above the Ionization Limit, *Phys. Rev. Lett.* **43**, 921 (1979).
- [21] V. Kondratovich, J. B. Delos, N. Spellmeyer, and D. Kleppner, Classically forbidden recurrences in the photoabsorption spectrum of lithium, *Phys. Rev. A* **62**, 043409 (2000).
- [22] T. W. Ducas, M. G. Littman, R. R. Freeman, and D. Kleppner, Stark Ionization of High-Lying States of Sodium, *Phys. Rev. Lett.* **35**, 366 (1975).
- [23] M. G. Littman, M. M. Kash, and D. Kleppner, Field-Ionization Processes in Excited Atoms, *Phys. Rev. Lett.* **41**, 103 (1978).
- [24] E. Luc-Koenig, S. Feneuille, J. M. Lecomte, S. Liberman, J. Pinard, and A. Taleb, Stark effect in quasi-hydrogenic species, *J. Phys. Colloq.* **43**, C2-153 (1982).
- [25] M. G. Littman, M. L. Zimmerman, and D. Kleppner, Tunneling Rates for Excited States of Sodium in a Static Electric Field, *Phys. Rev. Lett.* **37**, 486 (1976).
- [26] M. Førre and J. P. Hansen, Selective-field-ionization dynamics of a lithium  $m = 2$  Rydberg state: Landau-Zener model versus quantal approach, *Phys. Rev. A* **67**, 053402 (2003).
- [27] H. J. Silverstone, Perturbation theory of the Stark effect in hydrogen to arbitrarily high order, *Phys. Rev. A* **18**, 1853 (1978).
- [28] C. Bordas and H. Helm, Electric-field ionization of Rydberg states of H<sub>3</sub>, *Phys. Rev. A* **47**, 1209 (1993).
- [29] A. A. Kamenski and V. D. Ovsianikov, Field dependence of the hydrogen Stark line intensities, *J. Phys. B* **33**, 491 (2000).
- [30] Y. Kayanuma, Population Inversion in Optical Adiabatic Rapid Passage with Phase Relaxation, *Phys. Rev. Lett.* **58**, 1934 (1987).
- [31] P. Ao and J. Rammer, Influence of Dissipation on the Landau-Zener Transition, *Phys. Rev. Lett.* **62**, 3004 (1989).
- [32] V. M. Akulin and W. P. Schleich, Landau-Zener transition to a decaying level, *Phys. Rev. A* **46**, 4110 (1992).
- [33] N. V. Vitanov and S. Stenholm, Pulsed excitation of a transition to a decaying level, *Phys. Rev. A* **55**, 2982 (1997).
- [34] C. A. Moyer, Quantum transitions at a level crossing of decaying states, *Phys. Rev. A*, **64**, 033406 (2001).
- [35] K. Saito, M. Wubs, S. Kohler, Y. Kayanuma, and P. Hänggi, Dissipative Landau-Zener transitions of a qubit: Bath-specific and universal behavior, *Phys. Rev. B* **75**, 214308 (2007).
- [36] R. Schilling, M. Vogelsberger, and D. A. Garanin, Nonadiabatic transitions for a decaying two-level system: Geometrical and dynamical contributions, *J. Phys. A Math. Gen.* **39**, 13727 (2006).
- [37] G. Dridi and S. Guérin, Adiabatic passage for a lossy two-level quantum system by a complex time method, *J. Phys. A Math. Gen.* **45**, 185303 (2012).
- [38] Y. Avishai and Y. B. Band, Landau-Zener problem with decay and dephasing, *Phys. Rev. A* **90**, 032116 (2014).
- [39] M. B. Kenmoe, S. E. Mkam Tchouobiap, C. Kenfack Sadem, A. B. Tchabda, and L. C. Fai, Non-adiabatic and adiabatic transitions at level crossing with decay: Two- and three-level systems, *J. Phys. A Math. Gen.* **48**, 095303 (2015).
- [40] For practical reasons we use the numerical solutions from MATHEMATICA software and use  $a_1(-1000) = 1 - a_2(-1000) = 1$ .
- [41] A. McCulloch, Y. Bruneau, G. Khalili, and D. Comparat, High-flux monochromatic electron and ion beams from laser cooled atoms, *Microsc. Microanal.* **20**, 1156 (2014).

- [42] K.-H. Weber and C. J. Sansonetti, Accurate energies of ns, np, nd, nf, and ng levels of neutral cesium, *Phys. Rev. A* **35**, 4650 (1987).
- [43] L. Wang, C. Li, H. Zhang, L. Zhang, Y. Yang, Y. Man, J. Zhao, and S. Jia, Using experimental measurements of three-level avoided crossings to determine the quantum defect for the Stark map of highly excited cesium Rydberg atoms, *Phys. Rev. A* **93**, 033416 (2016).
- [44] J. Deiglmayr, H. Herburger, H. Saßmannshausen, P. Jansen, H. Schmutz, and F. Merkt, Precision measurement of the ionization energy of Cs i, *Phys. Rev. A* **93**, 013424 (2016).
- [45] R. G. Hulet and D. Kleppner, Rydberg Atoms in “Circular” States, *Phys. Rev. Lett.* **51**, 1430 (1983).
- [46] C. H. Cheng, C. Y. Lee, and T. F. Gallagher, Production of Circular Rydberg States with Circularly Polarized Microwave Fields, *Phys. Rev. Lett.* **73**, 3078 (1994).
- [47] J. Hare, M. Gross, and P. Goy, Circular Atoms Prepared by a New Method of Crossed Electric and Magnetic Fields, *Phys. Rev. Lett.* **61**, 1938 (1988).
- [48] S. N. Pisharody, J. G. Zeibel, and R. R. Jones, Imaging atomic Stark spectra, *Phys. Rev. A* **61**, 063405 (2000).
- [49] S. Feneuille, S. Liberman, J. Pinard, and A. Taleb, Observation of Fano Profiles in Photoionization of Rubidium in the Presence of a dc Field, *Phys. Rev. Lett.* **42**, 1404 (1979).
- [50] C. Chardonnet, D. Delande, and J. C. Gay, Generation of quasi-Fano profiles in the low field Stark spectrum of caesium, *Opt. Commun.* **51**, 249 (1984).
- [51] S. Feneuille, S. Liberman, E. Luc-Koenig, J. Pinard, and A. Taleb, Field-induced stabilisation of Stark states in the rubidium, *J. Phys. B* **15**, 1205 (1982).
- [52] J.-Y. Liu, P. McNicholl, D. A. Harmin, J. Ivri, T. Bergeman, and H. J. Metcalf, Interference Narrowing at Crossings of Sodium Stark Resonances, *Phys. Rev. Lett.* **55**, 189 (1985).
- [53] J. M. Lecomte and E. Luc-Koenig, Exact stabilisation versus approximate stabilisation of a Stark state through ionising-channel interference, *J. Phys. B* **18**, L357 (1985).
- [54] P. McNicholl, T. Bergeman, and H. J. Metcalf, Lifetime measurements of interference-narrowed sodium Stark resonances, *Phys. Rev. A* **37**, 3302 (1988).
- [55] C. Chardonnet, D. Delande, and J. C. Gay, Interference and stabilization in the quasibound Stark spectrum, *Phys. Rev. A* **39**, 1066 (1989).
- [56] A. Nussenzweig, E. E. Eyler, T. Bergeman, and E. Pollack, Line shapes of ionizing Stark resonances in helium, *Phys. Rev. A* **41**, 4944 (1990).
- [57] A. König, J. Neukammer, H. Hieronymus, and H. Rinneberg, Field-ionization Stark spectra of Ba Rydberg atoms at high density of states, *Phys. Rev. A* **43**, 2402 (1991).
- [58] A. S. Stodolna, F. Lépine, T. Bergeman, F. Robicheaux, A. Gijsbertsen, J. H. Jungmann, C. Bordas, and M. J. J. Vrakking, Visualizing the Coupling Between Red and Blue Stark States Using Photoionization Microscopy, *Phys. Rev. Lett.* **113**, 103002 (2014).
- [59] However, when the instabilities are incoherent, that is, when the decay occurs because of coupling to different continua, the Hamiltonian of the system is simply the lossy Landau-Zener system but with  $E_1(t)$  replaced by  $E_1(t) - i\hbar\Gamma_1/2$  [38].
- [60] X. Chen and J. A. Yeazell, Autoionization of a quasicontinuum: Population trapping, self-trapping, and stabilization, *Phys. Rev. A* **58**, 1267 (1998).
- [61] M. Eckstein, N. Mayer, C.-H. Yang, G. Sansone, M. J. J. Vrakking, M. Ivanov, and O. Kornilov, Interference stabilization of autoionizing states in molecular  $N_2$  studied by time- and angular-resolved photoelectron spectroscopy, *Faraday Discuss.* **194**, 509 (2016).